This is a peer reviewed, accepted author manuscript of the following article: Jelbuldina, M., Korganbayev, S., Korobeinyk, A. V., Inglezakis, V. J., & Tosi, D. (2018). Temperature profiling of ex-vivo organs during ferromagnetic nanoparticles-enhanced radiofrequency ablation by fiber Bragg grating arrays. In *40th Annual International Conference of the IEEE Engineering in Medicine and Biology Society, EMBC 2018* (Proceedings of the Annual International Conference of the IEEE Engineering in Medicine and Biology Society, EMBS; Vol. 2018-July). Institute of Electrical and Electronics Engineers Inc.. https://doi.org/10.1109/EMBC.2018.8513227

Temperature Profiling of *ex-vivo* Organs during Ferromagnetic Nanoparticles-Enhanced Radiofrequency Ablation by Fiber Bragg Grating Arrays

First A. Author, Second B. Author, Jr., and Third C. Author, *Member, IEEE*

***Abstract* — In this work, we report the real-time temperature profiling performed with a fiber Bragg grating (FBG) sensing system, applied to a ferromagnetic nanoparticles (NP)-enhanced radiofrequency ablation (RFA) for interventional cancer care. A minimally invasive RFA setup has been prepared and applied *ex vivo* on a liver phantom; NPs (with concentration of 5 mg/mL) have been synthetized and injected within the tissue prior to perform the ablation, in order to facilitate the heat distribution to the peripheral sides of the treated tissue. Temperature detection has been realized *in situ* with a network of 15 FBG sensors in order to highlight the impact of the NPs on the RFA mechanism. Obtained thermal profiles confirm that nanoparticles injection ensures better heat penetration than a standard RFA achieving an almost double-sized lesion. Thermal data are reported highlighting both spatial and temporal gradients, evaluating the capability of NPs to deliver sufficient heating to the peripheral sides of the tumor borders.**

I. Introduction

Radiofrequency thermal ablation (RFA) is widely used in clinical practice for minimally invasive treatment of kidney [1], hepatic [2, 3] and other types of tumors. Compared to more invasive surgical procedures, RFA makes use of miniature percutaneously inserted devices, which is a useful option for patients who are non-operative candidates, or have unresectable tumors.

RFA makes use of RF irradiance to generate thermal field confined to the proximity of an active electrode, which is shaped as a minimally invasive metallic applicator [3, 4]. The tissue acts as a load that dissipates the electrical power on the active part of the electrode; the surrounding parts of the tissue are then progressively heated following the heat transfer equations. As demonstrated in works [5, 6] an exposure to 52 °C for 60 s is considered a reference to ensure cancer cells mortality, while 60 °C is considered as the threshold for successful tumor necrosis in fast ablation phenomena.

Since tumor mortality rate is associated with the temperature at the ablation point, accurate measurement of tissue temperature is a key procedure for RFA. Moreover, it is necessary to achieve a dense thermal profiling *in situ*, in order to estimate the size of successfully ablated tissue. Current thermal monitoring techniques rely mostly on electrical thermocouples (TCs) [7, 8]; however, their slow response time and inability to provide sufficient sensing density limit application of thermocouples for RF thermal mapping. Another drawback is that thermocouples measure the temperature only in the region reached by RF applicator, rather than on the peripheral sides of the tumor. Fiber optic sensors based on fiber Bragg gratings (FBGs) present an effective alternative to perform high resolution temperature measurement [9]. FBG sensors are small in size, lightweight, biocompatible, and immune to electromagnetic field (including the field radiated on the RFA tip).

An inherent limitation of RFA is the steep rise of the tissue impedance when the ablation temperature reaches ~100 °C. At such a temperature the electrical resistivity of the tissue rises fast due to vaporization of the tissue water constituents [10, 11]. This effect interrupts the ablation procedures, preventing the heat to reach the outer borders of tumors, hence limiting the size of ablated tissue. In order to contrast this limitation, Tamarov *et al.* reported the use of Si nanoparticles (NP) [12], while Gannon *et al.* evaluated Au nanoparticles to mediate the ablation process [13]. Overall, the use of NP introduced *in situ* within the tissue alters the electrical impedance and the heat conductivity of the tissue, depending on their density and position [12]. Previous studies [13, 14] show that NP-mediated ablation has a better capacity of delivering heat to the peripheral sides of the tumors.

In this paper we propose a concept of ferromagnetic nanoparticles-enhanced RFA with *in-situ* thermal profiling. Magnetic nanoparticles (MNPs) for medical application are getting great attention of researchers. An application of MNPs in the RFA hyperthermia, a method in which tumor cells are treated with the heat generated from MNPs in a high frequency field is governed by Néel relaxation, Brownian relaxation, and a hysteresis loss mechanism [15]. Biocompatibility of various MNPs has been demonstrated both *in vitro and in vivo* [16-18].

To investigate the effectiveness of MNPs application in RF thermal ablation, we propose a configuration of 15 FBG sensors, that allows detecting the temperature in multiple points in real time. The results presented as thermal maps, i.e. temperature as a function of space and time, demonstrate real time temperature distribution and therefore the size of the ablated tissue can be estimated.

Research supported by ORAU project LIFESTART.

X. Y. are with Nazarbayev University, School of Engineering, 010000 Astana, Kazakhstan (e-mail: XXX)

X. Y. are with National Laboratory Astana, Laboratory of Biosensors and Bioinstruments, 010000 Astana, Kazakhstan.

II. MATERIALS AND EXPERIMENTAL SETUP

A. Thermal ablation setup

A schematic view of the thermal ablation setup and FBG sensory system is plotted in Fig. 1. The RF probe is a single-tip solid brass percutaneous device of 16 cm in length and 0.3 cm diameter, and terminated with a conical active electrode

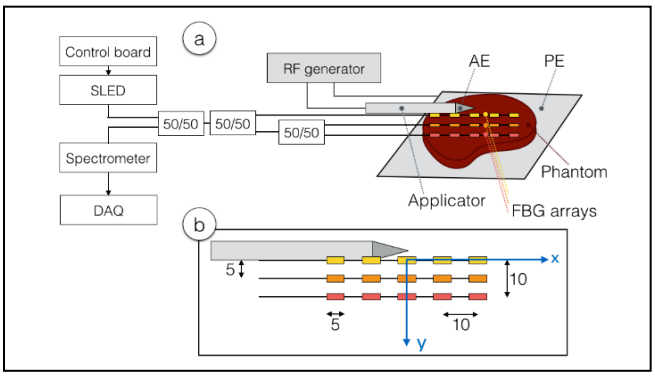

(AE) with 0.5 cm length; a metallic plate positioned

Fig. 1. Setup of the RFA thermotherapy and FBG measurement setup. (a) Schematic of the setup (SLED = superluminescent light emitting diode; DAQ = data acquisition; AE = active electrode; PE = passive electrode). (b) The insert shows the position of the 15 FBGs arranged in 3 arrays within the *xy* plane and relative to the RFA tip. Numbers refer to the distances in mm.

underneath the tissue serves as a passive electrode (PE). The RF probe is powered by a 450-kHz generator (RFA Hybrid Generator, Leanfa s.r.l.). The RF power has been set to 50 W for all experiments. Experiments were carried *ex vivo* on a porcine liver phantom, in agreement with EU protocols [19, 20]. A liver sample was held at room temperature (~ 20 °C) before the start of the experiment.

B. FBG measurement setup

The sensing system is realized by a network of FBGs. An FBG is a periodic modulation of the refractive index within the core of a single-mode silica optical fiber [21] which creates a resonant condition at the so-called Bragg wavelength. For an FBG having a modulation period Λ and effective refractive index n_{eff}, the Bragg wavelength $\lambda_{B,0}$ in reference condition is given by:

$$\lambda_{B,0} = 2n_{eff}\Lambda \tag{1}$$

The FBG sensing mechanism is based on λ_B shift due to variation of modulation period and effective refractive index. These variations are caused by changes in external parameters, like temperature and strain. Consequently, a temperature variation ΔT results in a linear shift $\Delta\lambda$ of the FBG spectrum, assuming a zero contribution of strain, and can be detected by a suitable peak-tracking method [22]:

$$\Delta\lambda = k_T \Delta T \tag{2}$$

where the temperature sensitivity coefficient is k_T.

Temperature sensing is accomplished with 15 FBGs inscribed in 3 ormoceramic optic fibers. Each fiber has 5 FBGs with 5 mm length and 10 mm distance between each FBG center. Fig. 1(b) inset shows positioning of each FBG sensor on a *xy* plane relative to the RF applicator; x is parallel to the applicator; the axis origin is the RFA tip. The central sensors (third element of each array) are aligned with the probe tip (x = 0 mm), while the other sensors are located at x = ±10 mm and x = ±20 mm from the probe tip. The sensor arrays are placed at a distance of y = 0 mm, y = 5 mm and y = 10 mm respectively from the applicator. Such configuration is a significant improvement compared to previous designs [11] as it allows the investigation of heat propagation in different directions and determining the size of ablated areas around the RFA tip.

All FBG arrays have been inserted in the phantom by using a percutaneous 22-Gage catheter [19, 20] that is pulled back after the insertion in order to leave the fiber *in situ*.

The interrogation setup is a custom-made system assembled into a portable case. It is based on a white light superluminescent LED source (SLED, Exalos EXS2100, 20 mW emission power) controlled by a driver board, and a low-cost infrared spectrometer as a detector (Ibsen I-MON-512-USB, 1520-1600 nm wavelength). A network of three 50/50 couplers has been used to route light to all sensor arrays and collect the backreflected spectra. This setup allows detecting the spectrum of the whole matrix of 15 FBGs, exploiting the wavelength division multiplexing [11]. All FBGs of the setup have different wavelength, with ~2 nm spacing between each adjacent wavelength: this spectral spacing is sufficient to avoid overlap of FBG spectra during sensing. Data acquisition and recording has been performed with a LabVIEW code that acquires the FBG spectra and estimates all the Bragg wavelengths; the peak tracking method is the spline as detailed in [22] which has a good accuracy (~1 pm) despite the coarse wavelength resolution and allows fast operation (close to 100 Hz). The thermal sensitivity of all ormoceramic FBGs is k_T = 10.2 pm/°C, calibrated as in work in Ref. [11] and very close to the manufacturer's specifications (10.1 pm/°C).

C. Nanoparticle synthesis

All chemical used are analytical grade and were purchased from Sigma-Aldrich. Magnetite nanoparticles (MNPs) of ~15 nm were synthesised by chemical precipitation of an aqueous solution containing Fe^{2+} ($FeSO_4 \cdot 7H_2O$, 99%) and Fe^{3+} ($FeCl_3 \cdot 6H_2O$, 97%) salts in the molar ratio Fe^{2+}/Fe^{3+} = 0.5 with sodium hydroxide (NaOH, 1.0 M). The synthesis was conducted on the 80° C hotplate. NaOH was added to iron solution with a fine rate of addition at 5 ml/min using an automatic burette. The solution was continuously stirred until pH reached 12. The precipitate was then centrifuged, washed several times with DI water and dried in an oven at 105°C for 8 hours.

In this work we directly injected magnetic particles into the extracellular space of tumor [23] in order to improve

MNPs distribution within the tumor (also in case of tumor with an irregular shape multiple-site injections can be exploited to cover the entire target region). For all ablation experiments, magnetite particles were dispersed in chitosan solution (0.5 wt%, in 1.0% acetic acid, Sigma-Aldrich) and a dose of 0.1 mL was injected into the phantom using a syringe.

III. EXPERIMENTAL RESULTS

We present results of the thermal ablation in absence of NP and enhanced with MNPs of 5 mg/mL concentration. The results of thermal profiling are illustrated, reporting the temperature recorded by each individual FBG, highlighting its *xy* coordinates and the 60 °C damage threshold [5] and thermal maps presented as contour charts of the temperature as a function of space and time. Central position of each sensor in the chart is reported as (*x*, *y*). The first experiment has been performed in absence of nanoparticles; the temperature traces are shown in Fig. 2(a) in the time domain. The experiment duration is 154 s. As observed in [11], temperature rises rapidly in the inner part of the tissue reaching the 60 °C threshold after few seconds, and reaching a maximum value of 157.8 °C. Overall, after 100 s, temperature values appear to stabilize. Moving along *x*, only the FBG positioned in (-10, 0) mm reaches the damage threshold value, while at the peripheral side of the tissue we observe a heating pattern that does not reach the threshold.

Fig. 3(a) reports the thermal maps obtained for the NP-free experiment. This chart is effective in showing the propagation of heat on the ablation plane. After the initial rise, the temperature exhibits a fast growth near the ablation peak and then stabilizes. Heat is however still propagating on the border of the tissue, as the temperature field is still expanding for y = 10 mm when the procedure is discontinued. Overall, with this interpolation method we estimate that the size of tissue which reached damage threshold is 19 mm for y = 0 mm, 15 mm for y = 5 mm, and 12 mm for y = 10 mm.

Insertion of 0.1 mL of 5 mg/mL MNPs alters temperature profiles of RFA, which is depicted in Fig. 2(b). At first, we observe that the maximum heating is obtained on the FBG elements positioned in front of the RFA tip (x = 10 mm) rather than in the central position. This is due to the NP effect, that contribute to reduce the average electrical impedance of the tissue and support a heat propagation to the peripheral areas. The presence of NPs makes 8 FBG sensors out of 15 record temperature peaks higher than 60 °C. Overall we can observe that the cytotoxicity region has significantly expanded with respect to Fig. 2(a). The duration of the experiment is 172 s and is longer than previous ablation; this is in part due to the effect of the ferromagnetic material, that by reducing the average impedance [14] during the most intense RFA heating prevents early disconnections of the RFA power, with the consequence that the heat is delivered to the peripheral regions in a much deeper way.

This analysis is complemented by the thermal maps, shown in Fig. 3(b). Thermal fields are substantially enlarged with respect to Fig. 3(a), due to the beneficial effect of the NP. At y = 0 mm, the extent of the >60 °C is approximately 32 mm, and the same value is observed at y = 5 mm. At y = 10 mm the tissue extent exceeding the damage threshold is 24 mm, and overall the size of the ablated volume is approximately double than the previous one. We also observe that when the RF power is discontinued (174 s), the deeper part of the tissue recorded by the third FBG array has already started cooling, which appears to suggest that the system has

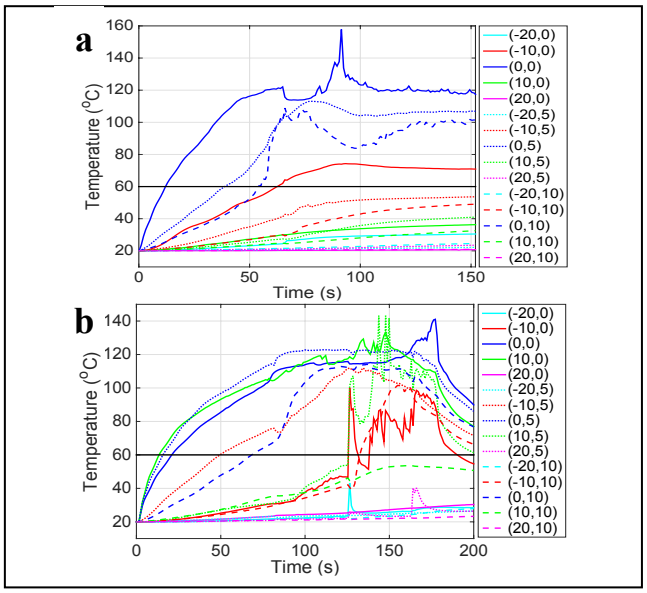

Fig. 2. Temperature recorded by each FBG for RFA experiments. The legend shows the (*x*,*y*) coordinate of each FBG in mm units. (a) Pristine ablation. (b) Ablation after 5 mg/mL MNPs injected.

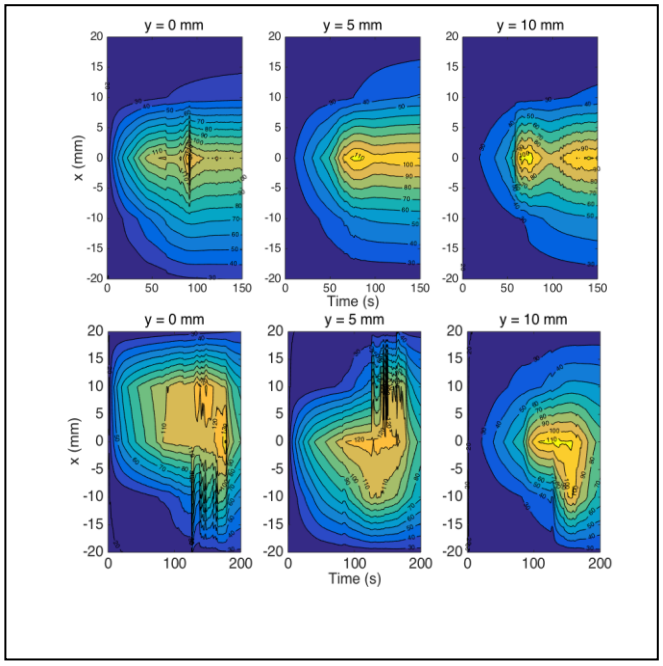

Fig. 3. Thermal maps for RFA experiments (a) in absence of NP, and (b) with MNPs concentration of 5 mg/mL. Data report the temperature level (in

°C) as a function of x and time for the first (left, y = 0 mm), second (center, y = 5 mm), and third (right, y = 10 mm) FBG arrays.

density of 5 mg/mL act as an enhancement of the ablation effect: heat is successfully spread to the peripheral sides of the tissue, a condition necessary to ablate larger tumors, and it has been possible to obtain a lesion >3 cm in diameter even with a single RFA applicator with one electrode.

IV. Conclusion

A conclusion section is not required.

References

[1] D. A. Gervais, F. J. McGovern, R. S. Arellano, W. S. McDougal, and P. R. Mueller, "Radiofrequency ablation of renal cell carcinoma: part 1, Indications, results, and role in patient management over a 6-year period and ablation of 100 tumors," *American Journal of Roentgenology,* vol. 185, pp. 64-71, 2005.

[2] L. Solbiati, T. Livraghi, S. N. Goldberg, T. Ierace, F. Meloni, M. Dellanoce*, et al.*, "Percutaneous radio-frequency ablation of hepatic metastases from colorectal cancer: long-term results in 117 patients," *Radiology,* vol. 221, pp. 159-166, 2001.

[3] J. P. McGahan and G. D. Dodd III, "Radiofrequency ablation of the liver: current status," *American Journal of Roentgenology,* vol. 176, pp. 3-16, 2001.

[4] S. Rossi, M. Di Stasi, E. Buscarini, P. Quaretti, F. Garbagnati, L. Squassante*, et al.*, "Percutaneous RF interstitial thermal ablation in the treatment of hepatic cancer," *AJR. American journal of roentgenology,* vol. 167, pp. 759-768, 1996.

[5] S. A. Sapareto and W. C. Dewey, "Thermal dose determination in cancer therapy," *International Journal of Radiation Oncology* Biology* Physics,* vol. 10, pp. 787-800, 1984.

[6] H. Rhim, S. N. Goldberg, G. D. Dodd, L. Solbiati, H. K. Lim, M. Tonolini*, et al.*, "Essential techniques for successful radio-frequency thermal ablation of malignant hepatic tumors," *Radiographics,* vol. 21, pp. S17-S35, 2001.

[7] M. Koda, S. Tokunaga, T. Matono, T. Sugihara, T. Nagahara, and Y. Murawaki, "Comparison between different thickness umbrella-shaped expandable radiofrequency electrodes (SuperSlim and CoAccess): Experimental and clinical study," *Experimental and therapeutic medicine,* vol. 2, pp. 1215-1220, 2011.

[8] S. O. Sofela, H. Younes, M. Jelbuldina, I. Saadat, and A. Al Ghaferi, "Carbon nanomaterials based TSVs for dual sensing and vertical interconnect application," in *Interconnect Technology Conference and 2015 IEEE Materials for Advanced Metallization Conference (IITC/MAM), 2015 IEEE International*, 2015, pp. 289-292.

[9] P. Saccomandi, E. Schena, and S. Silvestri, "Techniques for temperature monitoring during laser-induced thermotherapy: an overview," *International Journal of Hyperthermia,* vol. 29, pp. 609-619, 2013.

[10] E. G. Macchi, M. Gallati, G. Braschi, A. Cigada, and L. Comolli, "Temperature distribution during RF ablation on ex vivo liver tissue: IR measurements and simulations," *Heat and Mass Transfer,* vol. 51, pp. 611-620, 2015.

[11] D. Tosi, E. Macchi, G. Braschi, M. Gallati, A. Cigada, S. Poeggel*, et al.*, "Monitoring of radiofrequency thermal ablation in liver tissue through fibre Bragg grating sensors array," *Electronics Letters,* vol. 50, pp. 981-983, 2014.

[12] K. P. Tamarov, L. A. Osminkina, S. V. Zinovyev, K. A. Maximova, J. V. Kargina, M. B. Gongalsky*, et al.*, "Radio frequency radiation-induced hyperthermia using Si nanoparticle-based sensitizers for mild cancer therapy," *Scientific reports,* vol. 4, 2014.

[13] R. Mooney, E. Schena, P. Saccomandi, A. Zhumkhawala, K. Aboody, and J. M. Berlin, "Gold nanorod-mediated near-infrared laser ablation: in vivo experiments on mice and theoretical analysis at different settings," *International Journal of Hyperthermia,* vol. 33, pp. 150-159, 2017.

[14] X. Yang, "Science to Practice: Enhancing Photothermal Ablation of Colorectal Liver Metastases with Targeted Hybrid Nanoparticles," *Radiology,* vol. 285, pp. 699-701, 2017.

[15] R. E. Rosensweig, "Heating magnetic fluid with alternating magnetic field," *Journal of magnetism and magnetic materials,* vol. 252, pp. 370-374, 2002.

[16] L. Gu, R. H. Fang, M. J. Sailor, and J.-H. Park, "In vivo clearance and toxicity of monodisperse iron oxide nanocrystals," *ACS nano,* vol. 6, pp. 4947-4954, 2012.

[17] A. Tomitaka, A. Hirukawa, T. Yamada, S. Morishita, and Y. Takemura, "Biocompatibility of various ferrite nanoparticles evaluated by in vitro cytotoxicity assays using HeLa cells," *Journal of Magnetism and Magnetic Materials,* vol. 321, pp. 1482-1484, 2009.

[18] C. Shundo, H. Zhang, T. Nakanishi, and T. Osaka, "Cytotoxicity evaluation of magnetite (Fe 3 O 4) nanoparticles in mouse embryonic stem cells," *Colloids and Surfaces B: Biointerfaces,* vol. 97, pp. 221-225, 2012.

[19] G. Palumbo, A. Iadicicco, D. Tosi, P. Verze, N. Carlomagno, V. Tammaro*, et al.*, "Temperature profile of ex-vivo organs during radio frequency thermal ablation by fiber Bragg gratings," *Journal of biomedical optics,* vol. 21, pp. 117003-117003, 2016.

[20] D. Tosi, E. G. Macchi, M. Gallati, G. Braschi, A. Cigada, S. Rossi*, et al.*, "Fiber-optic chirped FBG for distributed thermal monitoring of ex-vivo radiofrequency ablation of liver," *Biomedical optics express,* vol. 5, pp. 1799-1811, 2014.

[21] A. D. Kersey, M. A. Davis, H. J. Patrick, M. LeBlanc, K. Koo, C. Askins*, et al.*, "Fiber grating sensors," *Journal of lightwave technology,* vol. 15, pp. 1442-1463, 1997.

[22] D. Tosi, "Review and Analysis of Peak Tracking Techniques for Fiber Bragg Grating Sensors," *Sensors,* vol. 17, p. 2368, 2017.

[23] I. Hilger, R. Hergt, and W. A. Kaiser, "Towards breast cancer treatment by magnetic heating," *Journal of Magnetism and Magnetic Materials,* vol. 293, pp. 314-319, 2005.